

## USING GAPS IN N-BODY TIDAL STREAMS TO PROBE MISSING SATELLITES

W. H. W. NGAN AND R. G. CARLBERG

Department of Astronomy and Astrophysics, University of Toronto, Toronto, ON, M5S3H4, Canada  
*Draft version December 12, 2017*

### ABSTRACT

We use N-body simulations to model the tidal disruption of a star cluster in a Milky-Way-sized dark matter halo, which results in a narrow stream comparable to (but slightly wider than) Pal-5 or GD-1. The mean Galactic dark matter halo is modeled by a spherical Navarro-Frenk-White (NFW) potential with subhalos predicted by the  $\Lambda$ CDM cosmological model. The distribution and mass function of the subhalos follow the results from the Aquarius simulation. We use a matched filter approach to look for “gaps” in tidal streams at 12 length scales from 0.1 kpc to 5 kpc, which appear as characteristic dips in the linear densities along the streams. We find that, in addition to the subhalos’ perturbations, the epicyclic overdensities (EOs) due to the coherent epicyclic motions of particles in a stream also produce gap-like signals near the progenitor. We measure the gap spectra – the gap formation rates as functions of gap length – due to both subhalo perturbations and EOs, which have not been accounted for together by previous studies. Finally, we project the simulated streams onto the sky to investigate issues when interpreting gap spectra in observations. In particular, we find that gap spectra from low signal-to-noise observations can be biased by the orbital phase of the stream. This indicates that the study of stream gaps will benefit greatly from high-quality data from future missions.

*Subject headings:* dark matter — galaxies: dwarf — galaxies: interactions — Galaxy: kinematics and dynamics

### 1. INTRODUCTION

The  $\Lambda$ CDM model – a universe dominated by cold dark matter and a cosmological constant – is a successful model of the universe at large scales (Blumenthal et al. 1984; Davis et al. 1985; Bardeen et al. 1986; Riess et al. 1998; Perlmutter et al. 1999; Planck Collaboration et al. 2013). However, as more observations are made and computational power becomes available, discrepancies in the model have been found below galactic scales. Cosmological simulations show that the dark matter halo of a Milky-Way-sized galaxy, in addition to having a smooth component with well-known density profiles (Navarro et al. 1997, 2004, 2010), should be populated by substructures, or subhalos (Madau et al. 2008; Stadel et al. 2009; Zemp et al. 2009; Springel et al. 2008; Gao et al. 2011). This theoretical prediction has not been supported by observational evidence, as many efforts over the past two decades have failed to find enough satellite systems in the Milky Way to account for the predicted abundance (Klypin et al. 1999; Moore et al. 1999; Strigari et al. 2007). This discrepancy is called the *Missing Satellite Problem*.

Competing solutions to the Missing Satellite Problem can be roughly classified into two types – astrophysical and physical. Astrophysical solutions, on one hand, postulate that the predicted subhalo abundance is correct, but the subhalos have too little stellar content to be observable directly. For example, reionizing radiation or stellar feedback (Koposov et al. 2009; Macciò et al. 2010) can suppress star formation in a subhalo. This class of solutions is founded on the absence of baryonic processes in those cosmological simulations which predicted the subhalo abundances. Phys-

ical solutions, on the other hand, postulate that the predicted subhalo abundance is incorrect, as our understanding of CDM may be incomplete. Alternative dark matter solutions, such as warm dark matter (Barkana et al. 2001; Bode et al. 2001; Benson et al. 2013; Schneider et al. 2013), self-interacting dark matter (Spergel & Steinhardt 2000), or inflationary models with non-scale invariance (Kamionkowski & Liddle 2000) offer mechanisms to suppress structure formation at small scales. Clearly, the predicted difference between these two types of solutions is the number of subhalos. In order to test the  $\Lambda$ CDM model at sub-galactic scales, measuring the true abundance of subhalos is an important step.

Tidal streams – or simply “streams” – are remnants of stellar systems such as globular clusters (GCs) or dwarf galaxies (DGs) as they are tidally disrupted by a massive host. When the stars become unbound from the progenitor, the stars trace an elongated tail which wraps around the massive host. Tidal remnants have long been useful probes for studying the gravitational potential of the Milky Way (e.g., Johnston 1998; Helmi et al. 2003; Law et al. 2005). In particular, Ibata et al. (2002) first used simulations to show that the encounters between the stream stars and subhalos can dynamically heat up the stream, which can be used to probe the presence of subhalos. Moreover, a key influence that subhalos have on streams is that the stream stars near the point of the encounter get scattered into different orbits by the perturbation, causing an abrupt decrease in stellar density in that region of an otherwise smooth stream. Using the abundance of subhalos obtained from high-resolution simulations (Madau et al. 2008; Springel et al. 2008), it has been predicted that streams in the Milky Way described by the  $\Lambda$ CDM model should contain many “gaps” (Yoon et al. 2011; Carlberg 2012; Carlberg et al. 2012;

Carlberg & Grillmair 2013).

In the past decade, many streams in the Milky Way have been found (see Grillmair (2010) for a list). Two streams of particular interest to us are Pal-5 (Odenkirchen et al. 2001) and GD-1 (Grillmair & Dionatos 2006). Both streams are detected as long, narrow tidal tails with length-to-width ratio of  $\sim 100$ . These two streams are interesting as they show varying densities longitudinally along the streams. It is not clear whether those density variations correspond to subhalo perturbations. Other possible origins of those density variations include clumping due to the coherence in the epicyclic orbits of stream stars (Küpper et al. 2008, 2010) and Jeans instabilities (Comparetta & Quillen 2011). The ultimate goal of this study is to test whether the gaps observed in streams are consistent with the prediction by the  $\Lambda$ CDM model. Yoon et al. (2011) and Carlberg (2012) independently made the first predictions by simulating ideal streams with massless particles in the presence of orbiting subhalos. In particular, Carlberg (2012) derived analytical expressions of the gap formation rate as a function of a stream’s intrinsic properties, which are readily comparable to observations. However, neither of the aforementioned studies self-consistently modeled the realistic disruption of the progenitor system.

In this study, we measure the gap formation rate by modeling a stream’s formation and its interaction with subhalos using N-body simulations. This paper is organized as follows. Section 2 describes the details of our simulations, including the subhalo abundances and density profiles that we adapt, and the details of the star cluster and the resulting model stream. Section 3 focuses on the method of detecting gaps in a simulated stream. The method of using match filters is inspired by analyses for observations, but modified here to analyze simulations. Section 4 contains detailed discussion of our key results, including the phenomenology of gaps and comparisons with previous analytical predictions and observations. Section 5 is a summary of our results.

## 2. SIMULATIONS

### 2.1. Models

The host galaxy is modeled as a dark matter halo, as well as a set of subhalos which orbit around the halo’s potential. A Milky-Way-sized halo is modeled with a static spherical Navarro-Frenk-White (NFW) profile (Navarro et al. 1997) with  $v_{max} = 210 \text{ km s}^{-1}$  located at  $r_{max} = 30 \text{ kpc}$ . Each individual subhalo is modeled by a spherical Hernquist profile (Hernquist 1990)

$$\Phi_i(r) = \frac{GM_i}{h_i + r} \quad (1)$$

for simplicity, compared to Einasto profiles which produce better fits in simulations but are more complicated to compute (Springel et al. 2008). We use the formula found in Carlberg (2009), which approximates the results from both Springel et al. (2008) and Neto et al. (2007), where  $h_i$  is independent of galactocentric position, and is related to  $M_i$  by

$$h(M) = 6 \text{ kpc} \times \left( \frac{M}{10^{10} M_\odot} \right)^{0.43}. \quad (2)$$

We use the mass and spatial distributions of the subhalos from the results of the Aquarius simulations (Springel et al. 2008), where the mass function is independent of the spatial distribution. The mass function is a power law

$$\frac{dN}{dM} = 3.26 \times 10^{-5} M_\odot^{-1} \left( \frac{M}{2.52 \times 10^7 M_\odot} \right)^{-1.9}, \quad (3)$$

and the spatial distribution follows an Einasto profile

$$n(r) \propto \exp \left\{ -2.95 \left[ \left( \frac{r}{199 \text{ kpc}} \right)^{0.678} - 1 \right] \right\}. \quad (4)$$

The subhalos’ velocities are initialized with a Gaussian distribution where the velocity dispersion is the solution to the isotropic Jean’s equation (Binney & Tremaine 2008) using the halo’s potential. The subhalos orbit around this potential as test masses.

The progenitor of the stream, which is an approximation to a globular star cluster, is initialized using  $10^6$  particles of equal mass as a King model with parameters  $w = 4.91$ , total mass  $4.29 \times 10^4 M_\odot$ , and a core radius of 0.01 kpc. This results in a zero-density radius of 0.103 kpc. Each N-body particle in the system interacts with the dark matter halo’s and subhalos’ potentials. With the Galactic center at the origin, the satellite is initially put at  $(x, y, z) = (30, 0, 0) \text{ kpc}$  and velocity  $(v_x, v_y, v_z) = (0, 140, 0) \text{ km s}^{-1}$ . The resulting orbit is confined on the  $xy$ -plane with eccentricity 0.33, peri- and apogalacticon at  $r_p = 15 \text{ kpc}$  and  $r_a = 30 \text{ kpc}$ , respectively. The azimuthal and radial periods are about 0.70 Gyr and 0.47 Gyr, respectively.

### 2.2. Software and Parameters

We use GADGET-2 (Springel 2005) for our N-body simulations. Since the public distribution<sup>1</sup> does not have functionality for external potentials, we modify the code such that in every time step, an external acceleration term which accounts for the potentials of the halo and all the subhalos is added to the accelerations of all the particles after their N-body interactions are computed.

Each of our simulations lasts 10 Gyr, and we impose a maximum time step of 1 Myr. The particle softening is 5 pc. Each simulation produces 500 snapshots, one every 20 Myr, and each consists of the positions and velocities of the N-body particles and subhalos.

### 2.3. Stream Properties

The star cluster is modeled as an N-body system which forms a stream as the cluster is disrupted by the tidal field of the massive host. When the cluster is isolated, the energies of the individual particles are conserved to a few percent over 10 Gyr. Using the softening as minimal impact distance, the relaxation timescale on the core is  $\gtrsim 110 \text{ Gyr}$ , which is much greater than the orbital period at  $\lesssim 1 \text{ Gyr}$ . Figure 1 shows the mass enclosed inside 0.103 kpc of the star cluster’s center it is orbiting in the absence of subhalos. Because the stream is repeatedly stretched and compressed longitudinally along the eccentric orbit, the mass enclosed in a fixed radius is not

<sup>1</sup> <http://www.mpa-garching.mpg.de/gadget/>

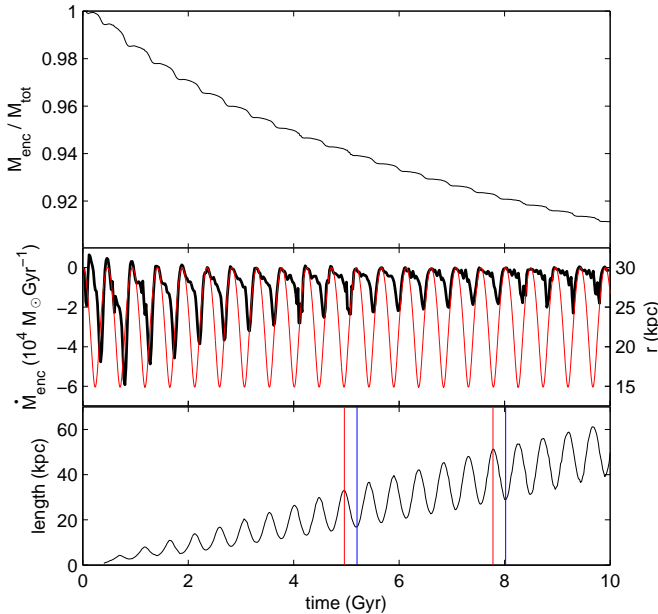


FIG. 1.— Top: fraction of mass enclosed in 0.103 kpc of the star cluster while orbiting the dark matter halo without any subhalos. Middle: rate of change of mass enclosed in 0.103 kpc of the star cluster (solid black) and radial position of the star cluster’s orbit (red). This shows that the star cluster experiences bursts of mass loss almost immediately after each pericentric passage. Bottom: length of the stream. This shows that the stream gets stretched and compressed depending on its orbital phase. The red and blue vertical lines correspond to the snapshots where the star cluster is at the pericenters and apocenters of its orbit, respectively. These times are selected to demonstrate the bias discussed in Section 4.4. always decreasing in time. The bottom panel of Figure 1 shows that the mass loss is driven purely by bulge shocking (Binney & Tremaine 2008), as the periodic bursts have exactly the same period as the radial period of the orbit.

Figure 2 shows the velocity dispersion and traverse FWHM of our simulated stream without any subhalos. The stream is chosen so that its properties are on the same orders of magnitude as Pal-5 (Dehnen et al. 2004; Odenkirchen et al. 2009) and GD-1 (Koposov et al. 2010; Willett et al. 2009). In the derivation in Carlberg (2012), the gap formation rate is expressed as a function of galactocentric distance of the orbit and width of the stream. For our simulated stream, we adapt average values of 22 kpc and 0.3 kpc, respectively, over the entire stream.

In a time independent and spherical potential  $\Phi(r)$ , three interesting conserved quantities are the radial, azimuthal, and latitudinal actions where

$$J_r = \frac{1}{\pi} \int_{r_p}^{r_a} dr \sqrt{2E - 2\Phi(r) - \frac{L^2}{r}} \quad (5)$$

$$J_\phi = L_z \quad (6)$$

$$J_\theta = L - |L_z| \quad (7)$$

respectively (Binney & Tremaine 2008), where  $r_a$  and  $r_p$  are the apo- and pericentric distances of the orbit, respectively. Since our stream’s orbital plane is the  $xy$ -plane,  $J_\theta \approx 0$  (though not exactly 0 because the stream has a finite thickness), so we only consider  $J_r$  and  $L_z$ . For simplicity, we ignore the progenitor and only consider the particles which have already escaped from the cluster, so

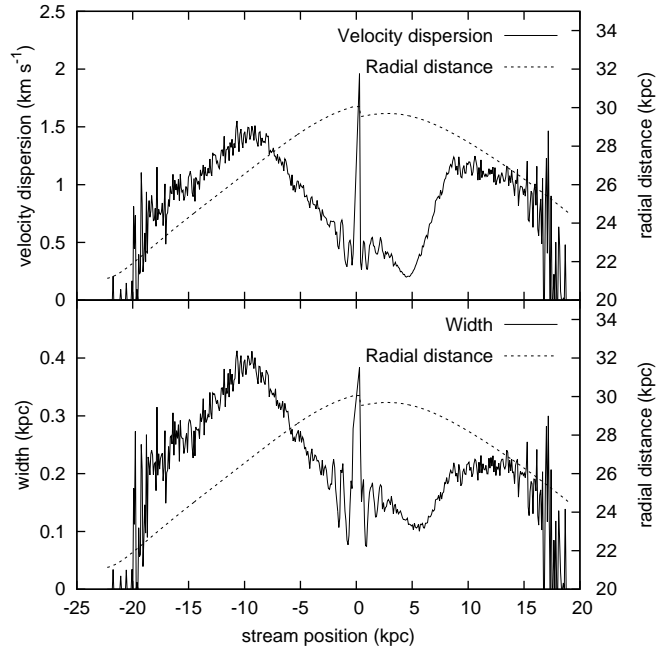


FIG. 2.— Tangential velocity dispersion and FWHM width along the stream at 8 Gyr. The progenitor is centered at 0 kpc, where positive and negative positions represent the leading and trailing branches of the stream, respectively. The structures in velocity dispersion and width are due to the eccentricity of the stream, as traced by the orbital distance along the stream.

when computing  $J_r$  we assume that the potential due to the progenitor’s potential is negligible.

$J_r$  and  $L_z$  are useful since their dispersions are the origins of the stream’s average width. For example, in the epicyclic approximation (Binney & Tremaine 2008) where  $\kappa$  and  $a$  are the epicyclic frequency and amplitude, respectively, the radial motion can be written as

$$r(t) = a \cos(\kappa t + \psi) \quad (8)$$

where  $\psi$  is an arbitrary phase angle. Then it can be shown that

$$J_r = \frac{1}{2\pi} \oint p_r dr \propto \int \dot{r} dr \propto \kappa a^2 \quad (9)$$

$$L_z = R_g^2 \Omega \quad (10)$$

where  $\Omega$  and  $R_g$  are the orbital frequency and radius of the guiding center, respectively. Clearly, dispersions in both  $a$  and  $R_g$  can affect the width of the stream. Therefore, conserved quantities  $J_r$  and  $L_z$  are especially valuable in understanding the width of the stream. Figure 3 shows the distributions in  $(J_r, L_z)$  when the stream is 8 Gyr old. The two lobes at higher and lower  $L_z$  are the trailing and leading branches of the stream, respectively. The absolute dispersions in  $J_r$  and  $L_z$  are on the same order of magnitude, in rough agreement with the formula  $\Delta J_r / \Delta L \sim (r_a - r_p) / \pi r_p$  (Eyre & Binney 2011). In Section 4.1, we will show how the spread in actions affects the morphology of stream gaps.

Plots similar to Figure 3 can be found in Eyre & Binney (2011) where they used angle-action variables extensively to study the relation between the stream and the orbit. A similar plot can also be found in Yoon et al. (2011), but in scaled energy and angular

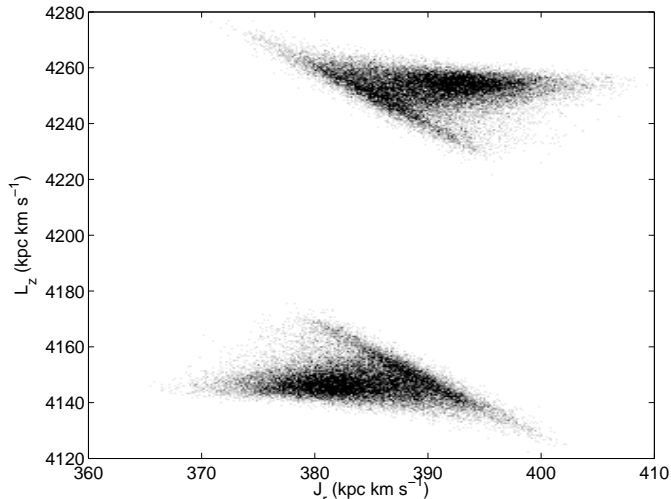


FIG. 3.— Distribution of orbital action variables ( $J_r$ ,  $L_z$ ) for our stream at 8 Gyr without any subhalos. Along the entire stream with the progenitor masked out, 50,000 unbound particles were randomly selected to be placed on this map. Each pixel in this map represents the density of particles in that bin. The two symmetric lobes are the two branches of the stream. Similar plots can be found in Eyre & Binney (2011), and a plot in scaled energy and angular momentum in Yoon et al. (2011).

momentum which were first used by Johnston (1998) to describe the dynamics of tidal streams.

### 3. METHOD

#### 3.1. Subhalo Mass Ranges

Yoon et al. (2011) divided their subhalo mass spectrum into separate mass ranges in order to resolve the contributions from each mass range. Using the same approach, we divide the subhalos from  $6.5 \times 10^4$  to  $10^8 M_\odot$  into 13 mass ranges (Table 1). Each mass range contains incrementally more subhalos, starting from the higher mass end toward the lower mass end. In the higher mass end, the mass ranges are chosen such that the increase in subhalo masses are roughly the same. In the lower mass end, the mass ranges are chosen such that the increase in subhalo numbers are roughly the same.

In each set of subhalos, we reduce their numbers by eliminating those whose orbits are always inside the perigalacticon and outside the apogalacticon of the progenitor’s orbit. The largest subhalo in our simulations has a length scale of  $\sim 1$  kpc (Equation (2)), so all the subhalos with perigalacticon (apogalacticon) larger (smaller) than that of the progenitor’s orbit by  $\sim 2$  kpc will interact minimally with the stream. This allows us to safely eliminate the subhalos with perigalacticon larger than 32 kpc, and apogalacticon smaller than 13 kpc.

We run 14 simulations – 1 “smooth stream” without any subhalos, and 13 “ $\Lambda$ CDM streams” containing the subhalos in the mass ranges in Table 1 – with identical initial conditions and dark matter halo potential. This allows us to resolve the effects of the lower mass subhalos whose existence are in question.

#### 3.2. Gap Finding

Gaps are manifested as local minima in the linear density along the stream. To obtain the linear density along a stream in an eccentric orbit, we first fit the stream with two degree-6 polynomials – one each for the leading and

TABLE 1  
THIRTEEN SUBHALO MASS RANGES IN OUR SIMULATIONS.

$m_{low}/M_\odot$	$N$	$M/M_\odot$	$N_{orbit}$	$M_{orbit}/M_\odot$
$5.3 \times 10^7$	203	$1.5 \times 10^{10}$	30	$2.2 \times 10^9$
$2.7 \times 10^7$	593	$2.9 \times 10^{10}$	98	$4.7 \times 10^9$
$1.3 \times 10^7$	1,392	$4.4 \times 10^{10}$	220	$6.9 \times 10^9$
$5.8 \times 10^6$	3,160	$5.9 \times 10^{10}$	476	$9.1 \times 10^9$
$2.5 \times 10^6$	7,038	$7.3 \times 10^{10}$	1,101	$1.1 \times 10^{10}$
$1.0 \times 10^6$	16,394	$8.8 \times 10^{10}$	2,576	$1.4 \times 10^{10}$
$3.6 \times 10^5$	41,515	$1.0 \times 10^{11}$	6,539	$1.6 \times 10^{10}$
$2.1 \times 10^5$	67,599	$1.1 \times 10^{11}$	10,563	$1.7 \times 10^{10}$
$1.5 \times 10^5$	91,601	$1.1 \times 10^{11}$	14,337	$1.8 \times 10^{10}$
$1.1 \times 10^5$	121,181	$1.2 \times 10^{11}$	18,872	$1.8 \times 10^{10}$
$9.0 \times 10^4$	145,220	$1.2 \times 10^{11}$	22,578	$1.9 \times 10^{10}$
$7.5 \times 10^4$	171,163	$1.2 \times 10^{11}$	26,586	$1.9 \times 10^{10}$
$6.5 \times 10^4$	194,726	$1.2 \times 10^{11}$	30,253	$1.9 \times 10^{10}$

The upper limit cuts off at  $10^8 M_\odot$  for all ranges. Columns from left to right: lower mass limit, total number and total mass in subhalos (Equation (3)), number and mass in subhalos used in simulation after reduction by orbit (see the text).

trailing streams – in polar coordinates centered at the Galactic center. The points along each line are spaced at 0.002 radians apart. Between each pair of adjacent points a cylinder of radius 1 kpc is drawn which lies lengthwise along the pair of points. The linear density is then the number of particles inside this cylinder divided by the length of the cylinder. This spacing is chosen so that the gaps as wide as the stream are well resolved.

The method used to find gaps in stream densities is inspired by the technique first used by Carlberg et al. (2012) to find gaps in observations. They used matched filters of the estimated shape of a density gap at various length scales to look for positions in the stream which potentially contain gap signals. The filter consists of a local minimum which is the underdensity of stars, and two local maxima on both sides of the minimum due to conservation of mass (Figure 4). This method is similar to the wavelets approach, where the integral of the filter function is constructed to vanish inside a certain domain. The potential gap signals are then easily identified as local maxima in the convolution between the filter and the signal.

To obtain the significance of each potential gap signal against noise, Carlberg et al. (2012) produced bootstrap samples from the sky background. With the simulations in this study, we can estimate noise levels using the smooth stream. Note that the “smooth stream” itself is not totally smooth. As we will show in Section 4.2, there are large density fluctuations near the progenitor due to the coherent in epicyclic motion of the particles, as first explained by Küpper et al. (2008). When the particles become unbound from the progenitor, they pile up near the base of their cycloid trajectories, creating epicyclic overdensities (hereafter EO) along the stream. Although this intrinsic process to mimic gaps can be confused with gaps caused by subhalos, EOs are only apparent within  $\lesssim 5$  kpc away from the progenitor in our streams (Figures 7 and 8). The details of the dynamics of EOs is beyond the scope of this study, but this effect can be understood in terms of orbital actions. EOs occur due to coherent epicyclic motions of the particles, which nevertheless have finite dispersions in orbital actions (Figure

3) and are not perfectly coherent. Therefore, although the escaping particles’ orbits stay roughly coherent in the first few clumps, their orbits eventually drift out of phase as they travel along the stream. This explains why the density peaks of EOs further downstream are not as apparent as the peaks closer to the progenitor (Just et al. 2009; Küpper et al. 2010).

After masking 10 kpc of the smooth stream centered at the progenitor, the rest of the smooth stream is simply noise. Our method to find gaps in a given stream can be summarized as follows.

### 1. Compute

$$C_s(x) = \frac{1}{s} \int_{x-1.5s}^{x+1.5s} [\rho(x') - \bar{\rho}_s(x)] f\left(\frac{2(x-x')}{s}\right) dx' \quad (11)$$

where  $f(t) = (t^6 - 1)\exp(-1.2321t^2)$  is a matched filter function (Carlberg et al. 2012; Carlberg & Grillmair 2013), and  $s$  is the filter scale.  $\bar{\rho}_s(x)$  is the mean of  $\rho(x)$  inside  $[x - 1.5s, x + 1.5s]$ , the domain in which the integral of  $f(2x/s)$  itself vanishes. Each potential gap signal would appear as a local maximum in  $C_s(x)$ . This convolution is computed at 12 logarithmically spaced filter scales from 0.1 to 5 kpc (Figure 4), and then all the local maxima of each stream are sorted by  $C_s$ .

2. Repeat the above step using the smooth stream, but with  $\pm 5$  kpc from the progenitor masked along the stream. The set of local maxima in  $\tilde{C}_s(x)$  from this convolution is the noise, which are also sorted by  $\tilde{C}_s$ .
3. Each local maximum in the signal set are compared against the noise set. A signal element at any position along either branch of the stream that ranks higher than 99% in the noise set is identified as a gap.

Inevitably, this method may detect the same gap at 99% confidence at different scales but in very close proximity. To avoid over-counting, we employ the following scheme to eliminate overlapping gaps. First, we define an overlap as two gaps whose  $C_s$  local maxima are identified at  $C_{s_1}(x_1)$  and  $C_{s_2}(x_2)$  that are within  $s_1$  away from each other along the stream, where  $s_2 < s_1$ . When this occurs, the gap with higher  $C_s$  eliminates the lower.

Our gap detection method requires no prior knowledge whether a given gap is an EO or a subhalo perturbation, both of which can be identified as a series of over- and under-densities. When we count the number of gaps in the end, EOs will be included. One key result of our study is that gaps due to EOs are distributed very differently in lengths compared to gaps due to subhalo perturbation.

## 4. RESULTS AND DISCUSSION

### 4.1. Gap Morphology

According to Yoon et al. (2011), gaps in general are diagonal and not perpendicular to the stream due to a gradient in angular momentum (hence a gradient in orbital velocities) across the width of the stream, which

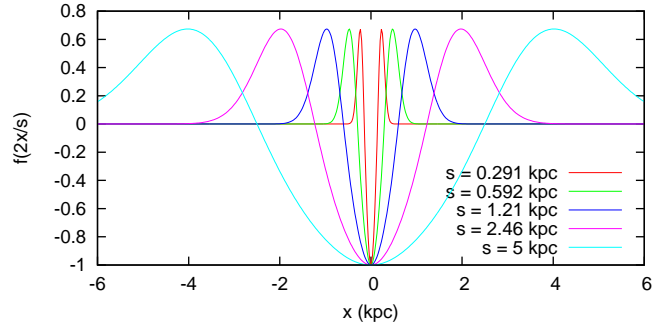


FIG. 4.— Five example filter scales for the match filter used in Carlberg et al. (2012), which has the functional form  $f(t) = (t^6 - 1)\exp(-1.2321t^2)$ . With a physical scale  $s$ , the integral of  $f(2x/s)$  vanishes inside  $-1.5s < x < 1.5s$ . The roots of each filter are located at  $\pm s/2$  so that the gap length is simply the distance between the roots. We search for gaps at 12 logarithmically filter scales from 0.1 to 5 kpc in order to minimize the chance of detecting the same gap at multiple scales.

can shear a gap longitudinally. Figure 3 allows us to estimate the shearing effect in our streams using the distributions in angular momenta. For each branch of the stream, the FWHM spread in angular momentum is about  $\Delta L \sim \Delta L_z \sim 10 \text{ kpc km s}^{-1}$ . For a narrow stream at  $r = 22 \text{ kpc}$ , the spread in velocity is  $\Delta v = \Delta L/r \sim 0.5 \text{ km s}^{-1}$ . Therefore, a gap that spans the width of the stream will be sheared by less than 1 kpc per Gyr.

Figures 5 and 6 show the time evolution of the smooth and a  $\Lambda$ CDM stream, respectively, from 7 to 8 Gyr. The EOs near the progenitor appear to shear by different amounts at different times, but this is due to the radial oscillation in the orbit where the radial period is  $\sim 0.5 \text{ Gyr}$ . Upon closer inspection of Figure 6, we also note that not only do subhalo gaps have complicated morphologies, but their orientations flip back and forth in a radial period due to the spread in  $J_r$ . Nevertheless, comparing panels of the same radial phase at one radial period apart, the end points of each gap across the width of the stream do not shift by any appreciable amount. Rather, the morphologies of the subhalo gaps are already apparent as each gap first appears.

If the linear density of a stream is calculated by integrating the entire thickness of the stream in traversing slices along the stream, then the contrast of the gap will be reduced. This is because the edges of the gaps are not perfectly straight across the width of the stream, so dividing the stream into slices will smear out the density contrast. To investigate how much the smearing will affect gap detection, we calculate the linear densities in two ways. (1) Integrating cylindrical slices of radius 1 kpc along the stream, hereafter the “whole width,” where 1 kpc was chosen to cover the entire thickness of the whole stream. (2) Integrating only the cylindrical slices of radius 0.04 kpc centered along the best fit line of each branch of the stream, hereafter the “central width,” where 0.04 kpc is chosen to mimic the GD-1’s observed width of 0.08 kpc (Carlberg & Grillmair 2013). This central width then encloses about 30%–40% of the mass of the whole width, depending on its orbital phase where, for example, the stream is radially compressed during pericentric passage.

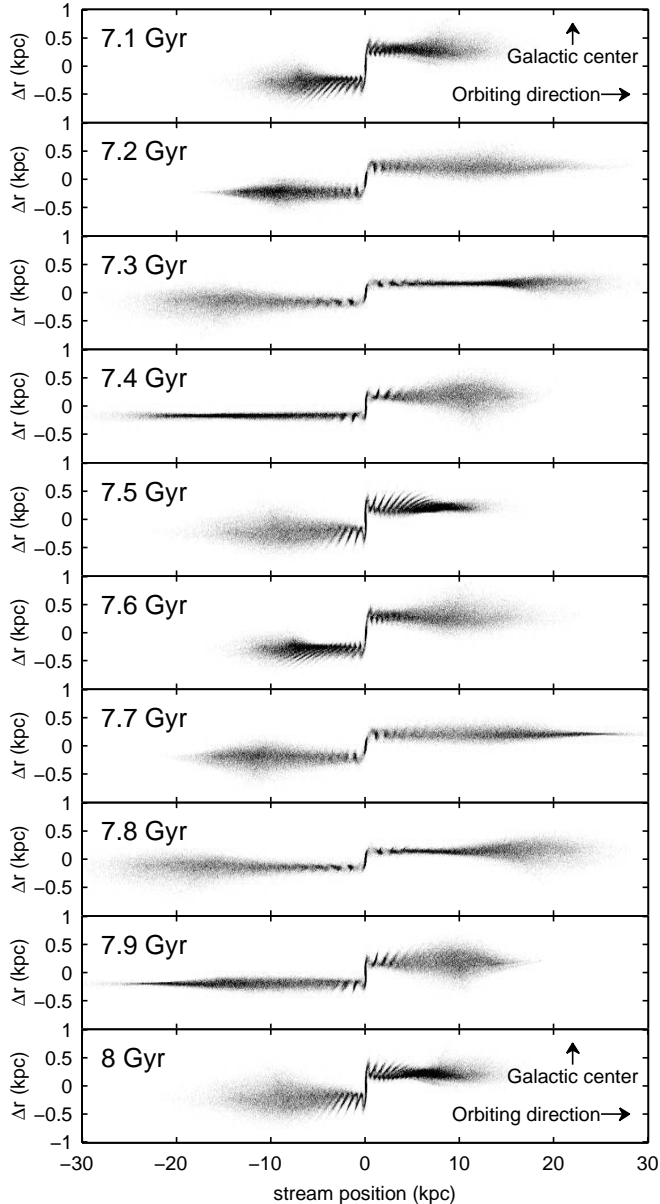


FIG. 5.— Surface density of the smooth stream from 7 to 8 Gyr projected onto the  $xy$ -plane. The stream is then aligned to Cartesian coordinates where the horizontal axis is the offset position along the stream from the progenitor, and the vertical axis is the radial offset from the galactocentric distance of the progenitor. This is done by tracing a best fit line along the stream. For each segment in the line, the particles in between the end points of the segment are rotated such that the Galactic center points toward the  $+y$  direction in this plot. Note that the vertical axis has been scaled 30 times the larger than the horizontal axis.

#### 4.2. Gap Counting

Figures 7–10 show the densities along the whole and central widths of the smooth stream and a  $\Lambda$ CDM stream from 3 to 10 Gyr. The streams younger than 3 Gyr are not shown as the stream is  $\lesssim 10$  kpc long at those ages, so the gaps are dominated by very prominent EOs. Moreover, the stream itself does not yet have a large enough cross section to produce enough gaps for meaningful statistics. In each panel, the shaded columns represent the gaps that are found on the scale of the columns’ widths. Although these gaps are identified as

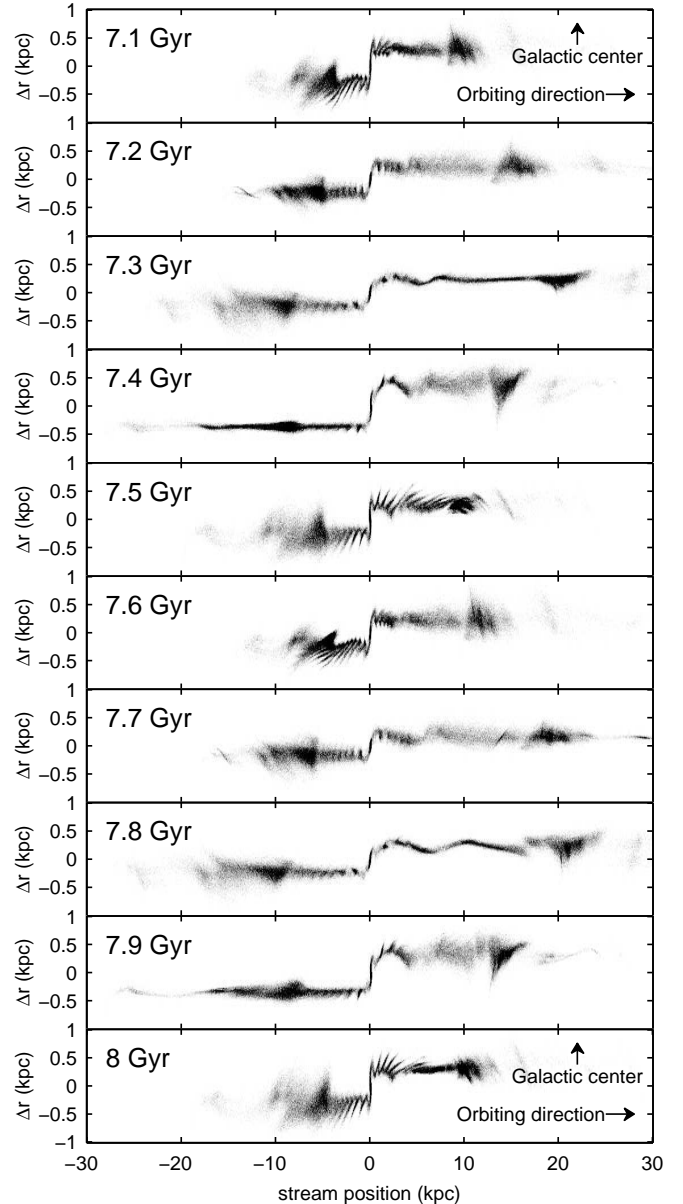


FIG. 6.— Stream with  $5.8 \times 10^6 < M/M_{\odot} < 10^8$  subhalos from 7 to 8 Gyr, aligned to Cartesian coordinates similar to the smooth stream in Figure 5. Compared to the smooth stream, this  $\Lambda$ CDM stream shows much more structures at various scales. In general, whether by EOs (mostly inside  $\pm 5$  kpc) or by subhalo perturbations, gaps have complicated morphologies and do not even have straight edges across the width of the stream.

being 99% significant, the density contrasts of the gaps have not been quantified. For the rest of this paper, we assume that all gaps identified at 99% significance can be observed. Note that because the gap finding process is applied independently to each snapshot, the shaded columns do not necessarily represent the time evolutions of individual gaps. Instead, the shaded columns show the general distributions of gaps – both in space and in gap lengths.

Our gap finding method has a number of problems. In the smooth stream (Figures 7 and 8), our method by construction identifies 1% of the noise as gaps. This is why there can be spurious gaps detected well beyond 5

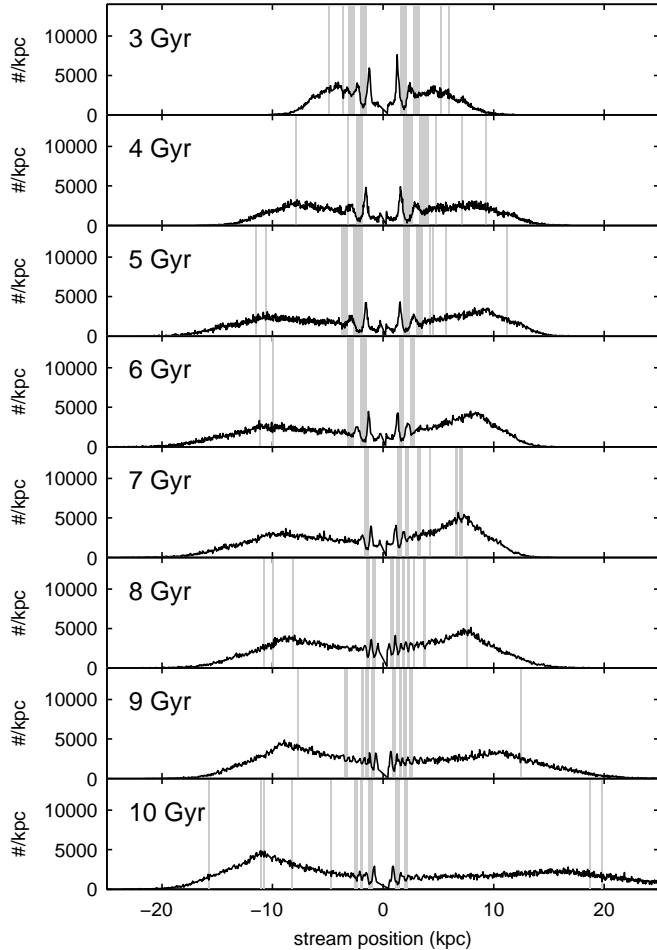


FIG. 7.— Linear densities along the smooth stream, integrated for the whole thickness of the stream, from 3 to 8 Gyr. The progenitor is centered at 0 kpc and is masked out. Shaded columns are gaps identified at 99% confidence at the scale depicted by the columns’ widths.

kpc away from the progenitor, even though EOs tend to form very close to the progenitor. Also, the overall profile of the stream density can sometimes be confused as a gap as well. One example is a gap at 4 kpc at 5 Gyr in Figure 9, where a smooth density gradient from 3 to 8 kpc is mistaken as the right half of a long gap. At the 95% confidence limit, both kinds of false positives are quite common and can often be identified by eye. For the results below, we show gaps that are 99% significant, which minimizes the occurrence false positives.

#### 4.3. Gap Spectrum

Following the idealized experiments in Carlberg (2012), Carlberg & Grillmair (2013) derived an analytical relation between gap formation rate  $R_{\text{U}}$  which is the cumulative number of gaps longer than length  $l$  per unit stream length per unit time as a function of gap length (hereafter the “gap spectrum”) such that

$$R_{\text{U}}^{\text{ideal}} = 0.060 \hat{r}^{0.44} l^{-1.16} \text{ kpc}^{-1} \text{ Gyr}^{-1} \quad (12)$$

where  $\hat{r} \equiv r/30 \text{ kpc}$ , and we adapt  $r = 22 \text{ kpc}$  for the average galactocentric radius of the stream. In this section we aim to study the validity of Equation (12) in our self-consistent stream. We set the “length” of each gap

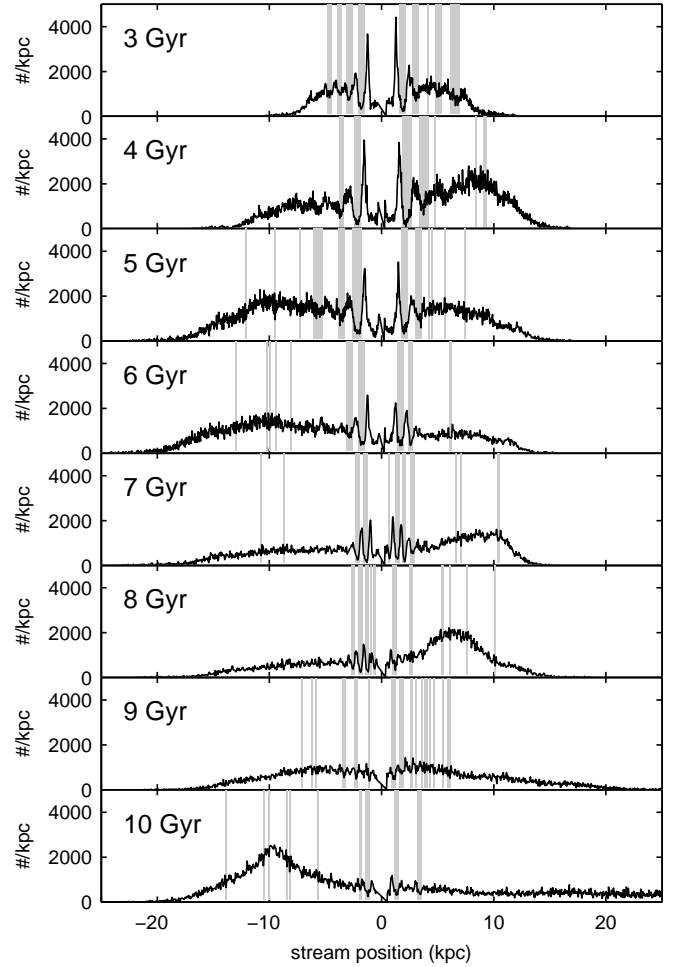


FIG. 8.— Linear densities and gaps identified at 99% in the smooth stream, but integrated for only a cylinder of diameter 0.08 kpc along the central line of the stream. as the scale  $s$  of the matched filter which identified the gap (Section 3.2)

##### 4.3.1. Smooth Stream without Subhalos

Figures 7 and 8 show the gaps identified in the smooth stream integrated using the whole thickness and central thickness, respectively. Clearly, the gaps due to EOs are clustered at  $\lesssim 5 \text{ kpc}$  on both sides of the progenitor, and all the gaps have very similar sizes. The measured  $R_{\text{U}}$  would peak at short gaps and quickly drops off beyond  $l \gtrsim 1 \text{ kpc}$ . Equation (12) is meant to describe an idealized gap spectrum produced by subhalos, and not by EOs.

A key result of this study, as discussed below, is that the gap spectrum for subhalo gaps looks very different than the gap spectrum for EOs. The existence of gaps longer than  $\sim 1 \text{ kpc}$  would be an indication that processes other than EOs are responsible for the gaps. Furthermore, subhalo gaps can be found everywhere along the whole stream. EOs can only be observed in the immediate vicinity of the progenitor.

##### 4.3.2. $\Lambda$ CDM Stream with Independent Sets of Subhalos

As an ideal case, Equation (12) ignores the visibility of gaps when the same position of a stream suffers impacts by multiple subhalos at different times. For instance, after one major impact by a massive subhalo which results

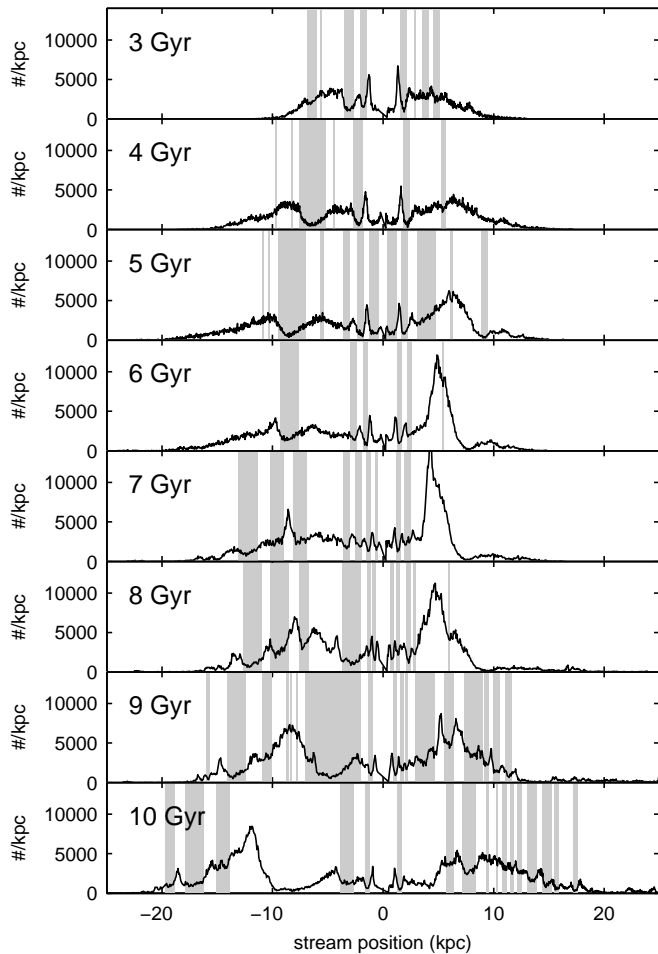


FIG. 9.— Linear densities and gaps identified at 99% in the  $\Lambda$ CDM stream with subhalo masses  $6.5 \times 10^4 < M/M_\odot < 10^8$ , integrated for the whole thickness of the stream.

in a long and high contrast density gap at an early time, subsequent impacts by less massive subhalos in that same region at a later time can not be visible.

Gap overlapping can be minimized by the following experiment. We run 13 separate simulations with the same initial conditions as the star cluster, but the subhalo masses are selected differentially from Table 1. This allows each stream to interact with an independent set of subhalos of a very small range of masses. Overlapping can still occur within the same simulation for each set of subhalos (hence a small number of gaps can still be eliminated), but to a much lesser extent than using integrated mass ranges.

Figure 11 shows the measured gap spectrum from the gaps collected from all 13 simulations using independent sets of subhalos. In the top panel which includes all gaps, the measured gap spectrum matches Equation (12) reasonably well. However, this is a coincidence as the gaps contain EOs which are not described by Equation (12). In an attempt to eliminate EOs, in the bottom panel of Figure 11, the gaps that are located within 5 kpc away from the progenitor are eliminated. When computing the gap formation rates in these cases, the number of gaps are divided by a stream length which is reduced by 10 kpc and a stream age which reduced by 2 Gyr (i.e., the age of the stream when it is 10 kpc long). This allows us to fa-

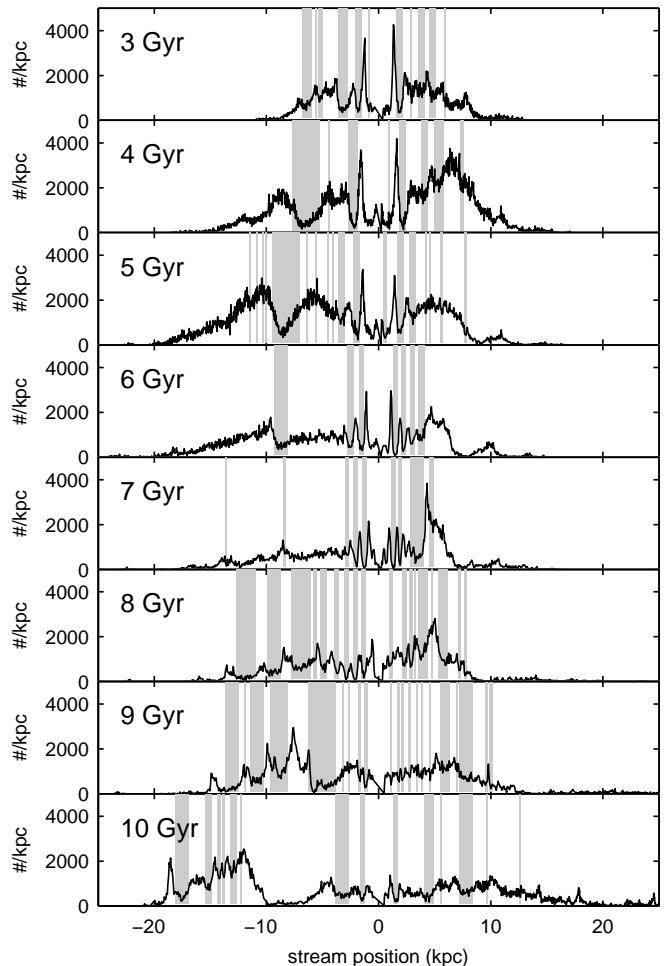


FIG. 10.— Linear densities and gaps identified at 99% in the  $\Lambda$ CDM stream with subhalo masses  $6.5 \times 10^4 < M/M_\odot < 10^8$ , integrate for only a cylinder of diameter 0.08 kpc along the central line of the stream.

ilitate a fair comparison of gap spectra against the cases which include all gaps in the entire stream. Comparing the two panels in Figure 11, we can see the masking of the 10 kpc around the progenitor reduces the abundance of shorter gaps. This is expected since that region of the stream contains mostly EOs which occur at scales  $\lesssim 1$  kpc. In general it is difficult to tell whether a given gap within 5 kpc is due to EOs or subhalos, so in the process some subhalo gaps near the progenitor may have been eliminated as well.

Whether Equation (12) is a good description of the gap spectrum in a general stream likely requires more simulations with varying orbital parameters. Nevertheless, it is apparent that the gap spectrum does not depend strongly on the age or the integrating width for the linear density of the stream. However, it is still an ideal case since a stream realistically interacts with all the subhalos at the same time. As we show in the following section, gap overlapping can significantly alter the gap spectrum.

#### 4.3.3. $\Lambda$ CDM Stream with all Subhalos

We now consider the validity of Equation (12) for stream gaps in the presence of all subhalos in each cumulative mass range in Table 1. Figure 12 compares the measured gap spectra of both the whole and cen-

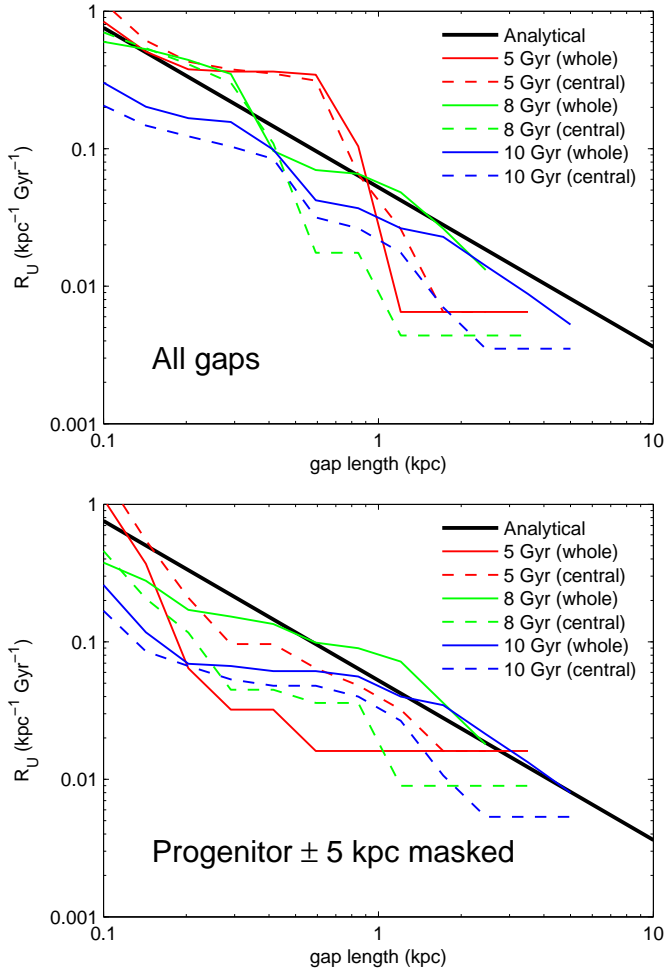


FIG. 11.— Analytical (Carlberg 2012) and simulated gap spectra. The gaps are collected from 13 simulations with independent sets of subhalos selected differentially from the mass ranges in Table 1. In the top panel, all gaps identified (including EOs) are included in the measured gap spectra. In the bottom panel, the gaps located within 5 kpc away from the progenitor are eliminated, and the stream lengths and ages are adjusted. Since the gaps are mostly independent, the gap spectra follow the analytical prediction reasonably well.

tral streams for three mass ranges, with and without the gaps within 5 kpc away from the progenitor. Clearly in all cases, the ideal gap spectrum over estimates the measured spectrum by nearly an order of magnitude due to gap overlapping.

Similar to the simulations with independent sets of subhalos (Figure 11), the gap spectra produced by full sets of subhalos do not have strong dependence on stream age and integrating width. The only exception is the youngest stream shown at 5 Gyr which consistently has higher  $R_U$  than the older streams. However, when the gaps near the progenitor are eliminated, the numbers of gaps at 5 Gyr in all cases decrease significantly, where the gap spectra are dominated by a single gap at 2–3 kpc, and a number of extremely short gaps. This is likely because the stream is still young, and the effective length of the stream (after masking 10 kpc centered at the progenitor) is only  $\sim 15$  kpc. This eliminates a significant part of the stream, making its stream statistics unreliable.

The weak dependence of the gap spectrum on the in-

tegrating width for linear density is also worth noting. Figure 6 shows that gaps in general have much more complicated morphologies than straight edges across the width of the stream. The explanation for these morphologies requires detailed understanding of how subhalo perturbations manifest in a self-consistent stream, which is beyond the scope of this study. While Carlberg (2013) studied the dynamics of subhalo perturbations for an idealized stream, we defer the self-consistent case to a future study.

Perhaps the most surprising result is that the gap spectra do not show obvious dependence on subhalo masses. The spectra are difficult to distinguish between the mass range of subhalos which causes the gaps. This is in disagreement with Carlberg (2012) which derived a relation between the length of a gap and the mass of the subhalo that caused it such that

$$l(M) = 8.3 \left( \frac{r}{30 \text{ kpc}} \right)^{0.37} \left( \frac{M}{10^8 M_\odot} \right)^{0.41} \text{ kpc}. \quad (13)$$

From this formula, it is reasonable to expect the inclusion of lower-mass subhalos to show more gaps at the shorter end. In their ideal simulations, however, Carlberg (2012) did not account for the time evolution of each gap. An example can be seen in Figures 9 and 10. The gap located at about  $-7$  kpc at 4 Gyr evolves into a much longer gap centered at about  $-9$  kpc at 10 Gyr. Evidently Equation (13) requires revision for self-consistent streams before it can be used to understand the relation between gap spectra and subhalo masses.

#### 4.4. Observational Considerations

We now consider the issues when interpreting gap spectra from observations. A gap spectrum for GD-1 has been observed by Carlberg & Grillmair (2013), but we emphasize that the gap spectra from our simulated streams in this study should not be directly compared to the one in Carlberg & Grillmair (2013) because our models for both the star cluster and the galaxy halo are chosen in favor of a simple interpretation, and may be missing some complications discussed in Section 4.6.

We first project each stream onto sky coordinates. For simplicity, we put the hypothetical observer at the center of the galaxy, and then project each particle onto the azimuthal and altitudinal plane in galactocentric coordinates. Since the our stream progenitor is orbiting along the  $xy$ -plane in a spherical potential, the smooth stream appears as a straight line along the azimuthal direction, and each  $\Lambda$ CDM stream appears only a few degrees off the azimuthal plane due to subhalo perturbations.

The density along the stream is simply the number of particles in bins of  $0.1^\circ$  in the azimuthal direction. The match filter approach to detect gaps remain the same as the analysis above, but the 12 filter scales (Figure 4) are now logarithmically spaced in angular units from  $0.34^\circ$  to  $14^\circ$ , and the noise levels are obtained from the regions at  $> 10^\circ$ , rather than  $> 5$  kpc, away from the progenitor. The choice of bin size and filter scales are on the same orders of magnitude as Carlberg & Grillmair (2013), but putting the hypothetical observer at the Galactic center may affect angular sizes by factors of  $\sim 2$ .

To ensure that the behaviors of the simulated streams are typical, we simulate each  $\Lambda$ CDM stream 10 times

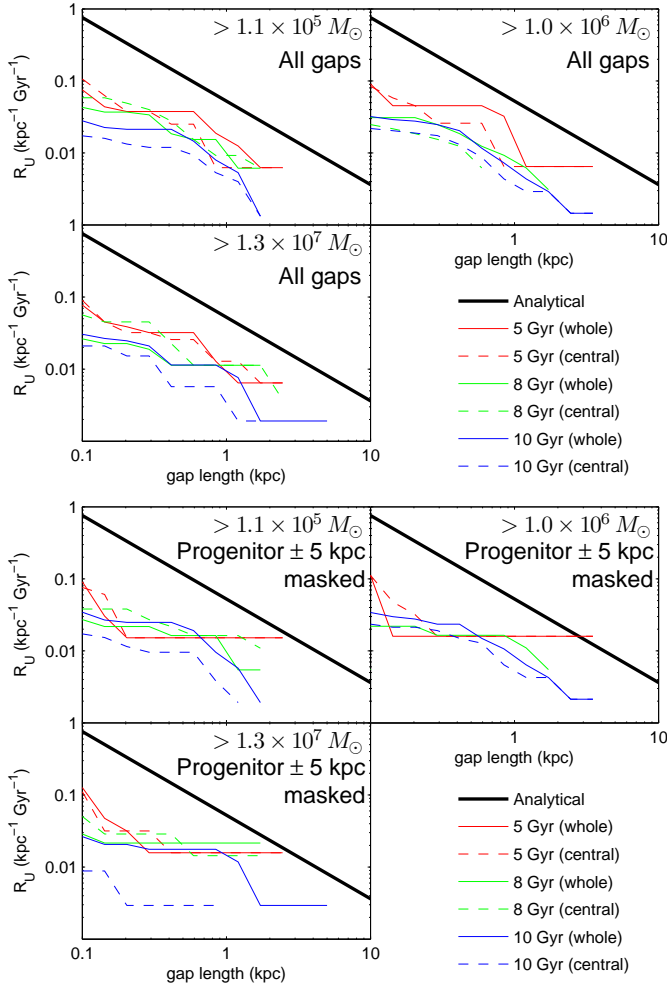


FIG. 12.— Analytical (Carlberg 2012) and simulated gap spectra. The gaps are collected from single simulations which include the full ranges of subhalos. The lower limit of the mass range is labeled in each panel, and the upper limit is  $10^8 M_\odot$  in all cases. In the top three panels, all gaps identified (including EOs) are included in gap spectrum. In the bottom three panels, the gaps located within 5 kpc away from the progenitor are eliminated, and the stream lengths and ages are adjusted. Compared to Figure 11, the simulated gap spectra here no longer follow the analytical prediction because of overlapping between the gaps.

with the same initial conditions for the star cluster, but different realizations of the same subhalo distributions. At the end we take the median numbers of gaps of the 10 streams to avoid outliers.

#### 4.4.1. Orbital Phase

One surprising result from Section 4.3.3 is that the gap spectrum has little to no dependence on age and subhalo masses. To investigate what this means when interpreting observations, the top panel of Figure 13 shows the cumulative numbers of gaps longer than  $0.34^\circ$  (i.e., all gaps detected in the entire stream) as functions of time. At  $t > 5$  Gyr, the numbers of gaps due to subhalos vary according to the orbital phase of the stream progenitor. The “bursts” in numbers of gaps in the  $\Lambda$ CDM streams occur when the streams are stretched as they pass through the pericenters of their orbits. At  $t < 5$  Gyr, on the other hand, this correlation does not exist for two reasons. First, our detection method (Section 3.2) uses the parts of the stream that are  $> 5$  kpc (before sky

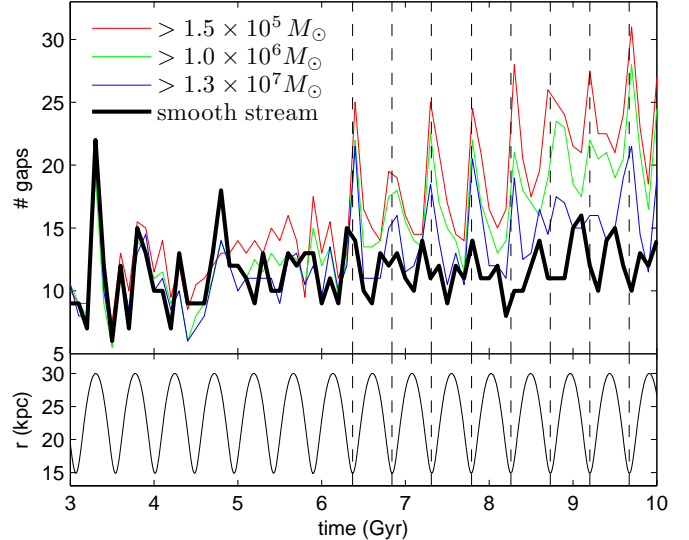


FIG. 13.— Top: time evolution of the number of gaps longer than  $0.34^\circ$ . Each colored line represents the median of 10 realizations of an identical subhalo distribution (with  $10^8 M_\odot$  as upper mass limit), and the black thick line represents the smooth stream. Bottom: the vertical dashed lines are visual guides which show that the variation of the number of gaps is correlated with the orbital phase of the stream progenitor. These plots show that the cumulative number of gaps in a stream on average is increasing in time, but instantaneously the number of gaps observable can have an even stronger dependence on the orbital phase of the stream than on the stream’s dynamical age or subhalo masses.

projection) or  $> 10^\circ$  (after sky projection) away from the progenitor in order to estimate noise. At  $t < 5$  Gyr, the length of the stream varies between a few to 20 kpc, which may not be long enough to estimate noise. Second, in only 5 Gyr the stream does not yet have enough time and to interact with subhalos.

Both the total number of gaps and the dynamical age of the stream are difficult to measure, as the some parts of a stream may not be observable. We define a more useful quantity  $S_U$  which is the cumulative number of gaps longer than a given gap length per unit stream length. In other words, leaving the age of the stream as an unknown,  $S_U$  differs from  $R_U$  in Section 4.3 by a normalization by age, and that  $S_U$  is after sky projection. In the next section we show that gaps due to EOs and subhalos have very different  $S_U(l)$  distributions which are directly observable.

#### 4.4.2. Signal-to-noise Ratios

Another important distinction between simulations and observations is the signal-to-noise ratio (S/N). At 5 and 8 Gyr our smooth stream is represented by about 60,000 and 80,000 particles in total, respectively (Figure 1). Koposov et al. (2010) estimated that the  $60^\circ$  visible segment of GD-1 consists of 3000 stars. At an average distance of  $\sim 10$  kpc, the visible segment is  $\sim 10$  kpc long. In our simulations, after 5 and 8 Gyr, the average stream lengths are about 20 and 40 kpc, respectively (Figure 1). This means that our simulated stream should be represented about eight times fewer particles in order to be comparable to observations. With the progenitor masked, we reduce the number of particles in the stream by randomly sampling the stream using two, four, and eight times fewer particles than the original stream. The particle reduction applies to both the stream of interest

and the smooth stream which is the source for estimating noise. This allows us to investigate the importance of high S/N.

Note that in our simulation each particle is equivalent to about  $0.043M_{\odot}$ , which is less massive than the typical stars that are detected in observations. Our simulations are not meant to be physical models of the real stream. In this section, we are only concerned about matching the numbers of particles in the simulations to the numbers of stars in the observation. As the stars escape from the progenitor, the stream’s self-gravity becomes negligible (Johnston 1998), and the particles’ masses are no longer important.

Figure 14 shows the density profiles of the  $\Lambda$ CDM stream with subhalo masses  $1.5 \times 10^5 < M/M_{\odot} < 10^8$  at 8 Gyr projected onto the sky. The panels show the gaps detected in the same stream after three levels of particle reduction. Even after reduction by a factor of eight, the stream appears to have retained most of its gaps despite a lower S/N.

In Figure 15, each line shows the median of ten gap spectra from the same stream but with 10 realizations of the same subhalo distribution. In each panel, the solid (dashed) lines represent the times when the progenitor is at the pericenter (apocenter) of its orbit. When the stream is compressed and stretched as it oscillates radially (see Figure 1), its length can differ by up to a factor of two. Careful inspection of Figures 13 and 15 shows that during pericentric passages, the numbers of gaps are at maximum, but  $S_{\perp}$  is at minimum because the stream length is also at maximum. For a  $\Lambda$ CDM stream at high S/N (upper left panel in Figure 15), the gap spectra are not sensitive to this oscillation, except with an excess of shorter gaps and fewer longer gaps, which are expected as the stream, including its longitudinal structure, is compressed during apocentric passage. At low S/N (lower left panel in Figure 15), however, the gap spectrum during apocentric passage is consistently higher than that during pericentric passage. This is because the length of the stream is insensitive to the S/N, but the number of gaps is not. Therefore, high S/N data for the stream is important when studying stream gaps. Otherwise, the spectrum may be over- or underestimated depending on the orbital phase.

The right panels in Figure 15 show the gap spectra of the smooth stream. They are also somewhat sensitive to S/N, but the most obvious difference from the spectra of  $\Lambda$ CDM stream is the shape of the spectra. This is especially obvious during pericentric passage where the gap spectra rapidly drop off to zero for gaps longer than  $\sim 1^{\circ}$ . Even during apocentric passage, the gap spectra remain flat at gap lengths  $\gtrsim 1^{\circ}$ . If the gaps originated from subhalo perturbations, then the gap spectrum should be steep and extend well beyond  $1^{\circ}$ .

#### 4.4.3. The Case of GD-1

An interesting confusion for GD-1 in particular is that GD-1’s progenitor has not been identified. If GD-1’s progenitor has evaded observation, and the observation corresponds to a segment of the stream which is close enough to the progenitor such that EOs can be observed, then GD-1 may be a poor choice as a probe for missing satellites. However, this is unlikely because EOs are observable only in a small segment of the stream, and subhalo

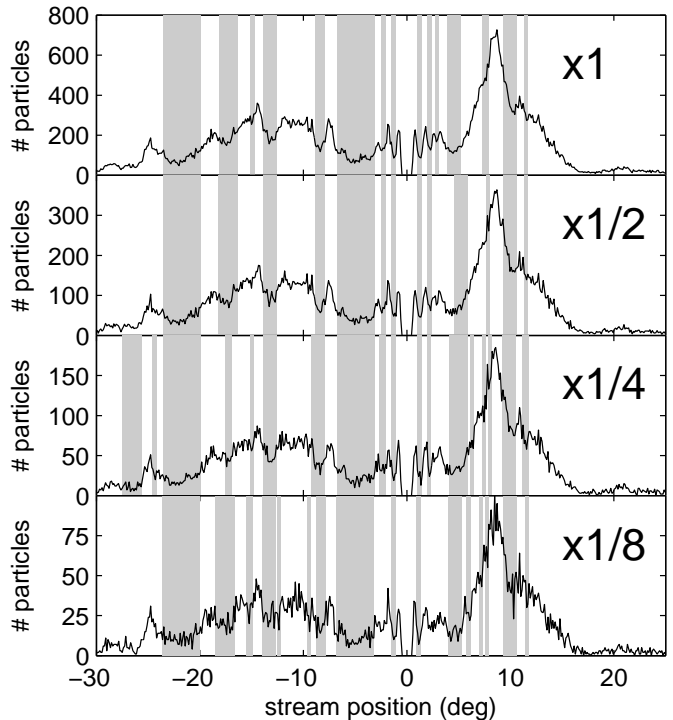


FIG. 14.— Density profiles and gaps detected at 99% confidence for the  $\Lambda$ CDM stream with subhalos of masses  $1.5 \times 10^5 < M/M_{\odot} < 10^8$  at 8 Gyr, projected onto the sky. Each panel represents a stream whose number of particles have been reduced by the factor indicated and binned at  $0.1^{\circ}$  throughout. Without reduction (top panel), the stream contains about 80,000 particles. The stream retains most of its gaps even after particle reduction by a factor of eight.

gaps are observable everywhere along the stream.

Another possibility is that GD-1’s progenitor may have been completely disrupted. In this case, the tidal radius of the progenitor approaches zero. Since the spacing between EOs are proportional to the tidal radius of the progenitor, this means that the EOs should also fade away as the progenitor is disrupted (Küpper et al. 2010). Therefore, despite its lack of progenitor GD-1 should be a viable probe for missing satellites.

The gap spectrum of GD-1 has been measured by Carlberg & Grillmair (2013). The spectrum show presence of gaps at all lengths between  $0.2^{\circ}$  and  $10^{\circ}$ , which is sufficient to rule out a smooth and spherical potential. To facilitate a conclusive analysis on the origin of the gaps in GD-1, we need to consider a much more realistic model which include the effects discussed in Section 4.6.

#### 4.5. Subhalo Mass Limits

We consider the effects of subhalos as massive as  $10^8 M_{\odot}$ , since the effects by more massive subhalos are not relevant to us. Gaps caused by subhalos at these masses produce long gaps with high-density contrasts. For example, an obvious gap located at  $-7$  kpc at 4 Gyr shown in Figures 9 and 10 are caused by a  $4.5 \times 10^7 M_{\odot}$  subhalo. In fact, the perturbation by  $M \gtrsim 10^8 M_{\odot}$  ( $h \gtrsim 1$  kpc) subhalos can be so catastrophic that the stream is warped and divided into segments. As a result, a stream which originated from one progenitor can be observed as a few separate streams. Observations of Pal-5’s and GD-1’s gaps, on the other hand, show small-

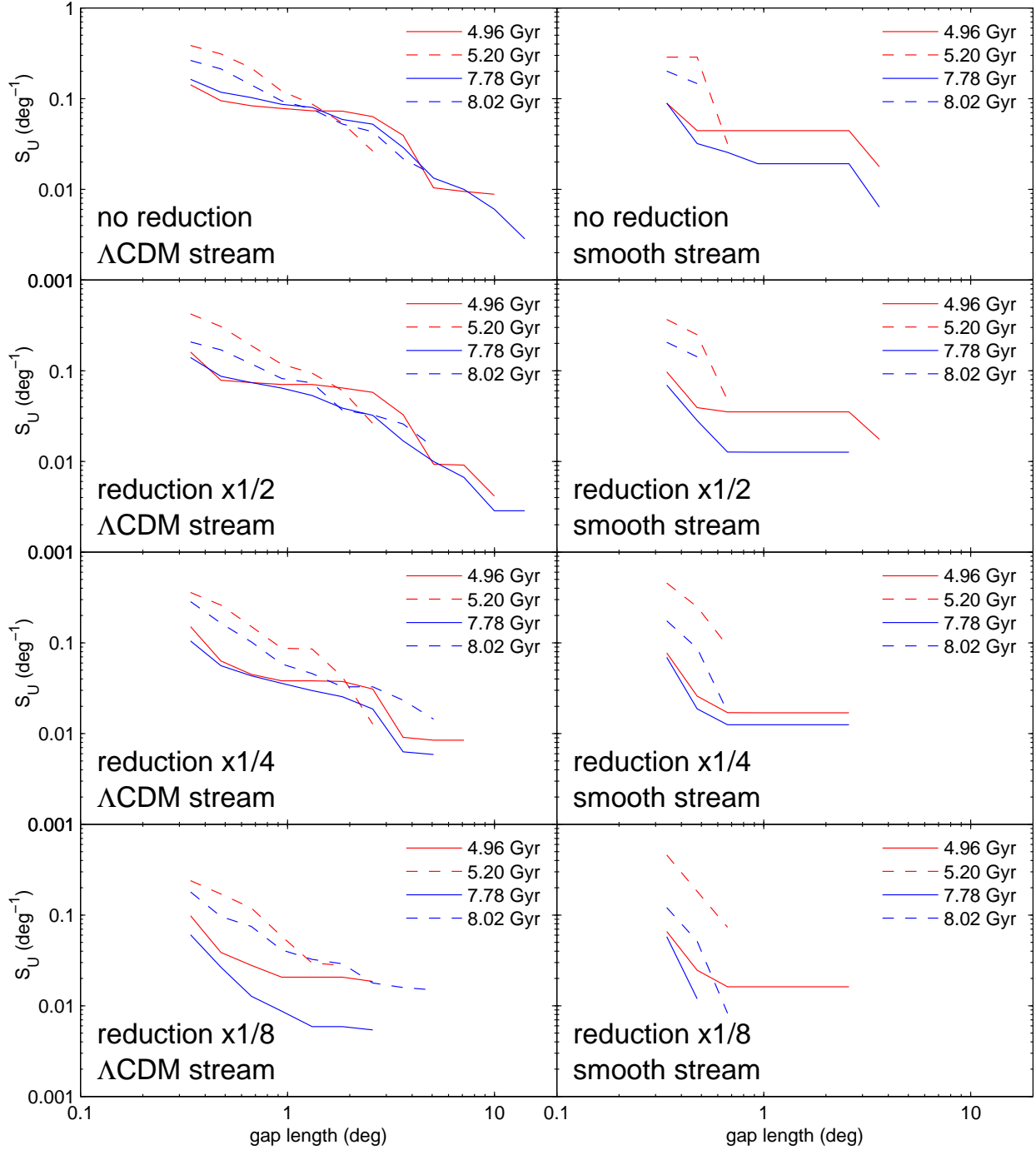


FIG. 15.— Gap spectra from simulated streams after sky projection. Each line in the panels on the left are the median of 10 spectra of the same  $\Lambda$ CDM stream but with ten identical subhalos distribution of masses  $1.5 \times 10^5 < M/M_\odot < 10^8$ . The panels on the right are the spectra of the smooth stream. The spectra of the  $\Lambda$ CDM stream show presence of gaps longer than  $1^\circ$ , whereas the spectra of the smooth stream quickly drops off. Colored solid (dashed) lines are spectra obtained when the stream is undergoing pericentric (apocentric) passage. Each row represents the spectra after the numbers of particles in the streams have been reduced by the factor labeled. The bottom panels indicate that a high S/N detection of the stream is important for understanding the origins of gaps, otherwise the gap formation rates can be systematically biased depending on the stream’s orbital phase.

scale density fluctuations in a long, narrow stream, so these two streams are not sensitive to subhalos above  $10^8 M_\odot$ . By coincidence, this upper limit approximately coincides with the upper limit beyond which the models of warm dark matter can be no longer distinguished from CDM. Therefore,  $10^8 M_\odot$  is a reasonable upper limit where our simulations can be useful.

In the low-mass end, we only consider the effects of subhalos down to  $\sim 6 \times 10^4 M_\odot$ . From a separate simulation of the same stream but with only the subhalos with masses  $6.5 \times 10^4 < M/M_\odot < 7.5 \times 10^4$ , the density profile is indistinguishable from the smooth stream, and the gap statistics are identical. Furthermore, Section 4.3.3 shows that the gap spectra have very little dependence on mass. Changing the mass lower limit from  $7.5 \times 10^4 M_\odot$  to  $6.5 \times 10^4 M_\odot$  produced indistinguishable gap spectra. This means that subhalos less massive than  $\sim 10^5 M_\odot$ , even though they are much more abundant than those of higher masses (Equation (3)), have minimal effects on our stream.

The Milky Way has about 160 known GCs (Harris 1996), and a few hundred DGs brighter than  $L \gtrsim 10^3 L_\odot$  after bias corrections (see Bullock (2010) for a review). It is interesting to ask whether these known satellite systems, rather than the truly “missing” satellites, can contribute to the observed stream gaps. Typical GCs have masses  $\sim 10^5 M_\odot$ , which correspond to the low end of our mass spectrum of subhalos. In the same mass range, though, there are orders of magnitude more subhalos (e.g.,  $\sim 10^5$  subhalos at  $10^5 < M/M_\odot < 10^6$ ) than GCs, so GCs are unlikely to contribute significantly to observed stream gaps. On the other hand, DGs are commonly found at  $\gtrsim 10^7 M_\odot$  (Strigari et al. 2008) which is the high end of our mass spectrum of subhalos. At that mass range ( $\sim 2000$  subhalos at  $M > 10^7 M_\odot$ ), the number of known DGs are only 1 order of magnitude below the number of subhalos, so DGs may contribute to some observed gaps. However, a common limitation in understanding the contributions from both GCs and DGs is their orbits, especially when the kinematics of these satellites are not well constrained. As done in our simulations (Section 3.1), subhalos that do not approach the stream’s orbit will interact minimally with the stream. Table 1 shows that in our realizations of subhalos, only  $\sim 15\%$  of them would approach to within 2 kpc of GD-1’s orbit. This means that most known satellites may never interact with a GD-1-like stream, and that stream gaps, if they were indeed due to satellites and were not EOs, are more likely due to satellites that have never been observed.

#### 4.6. Other Effects

In order to keep our results simple, the galaxy is modeled as stationary, spherical NFW potential, the subhalos as static, test masses, and the satellite as a collisionless King model. These models ignore a number of known dynamical complications.

*Two-body Relaxation.* The star cluster is modeled as a collisionless system with relaxation timescale of  $\sim 110$  Gyr. Globular clusters typically have relaxation timescales of  $\lesssim 10$  Gyr (Harris 1996, 2010 Edition), so mass loss should originate from dynamical evaporation, in addition to tidal disruption. As a result, the star cluster should be disrupted even faster than we measured

in Figure 1. This may have an important effect on the formation of gaps, which depends on the details of the dynamics of a stream (Carlberg 2013). The relation between gaps and mass loss mechanism will be investigated in a future study.

*Dynamical Friction (DF).* Both the star cluster and subhalos should suffer from DF as they orbit around the dark matter halo. Comparing the magnitudes of the accelerations due to DF and due to the orbit,  $a_{DF}/a_{orbit} \sim 10^{-8} \ln \Lambda$  for both the star cluster at 22 kpc and a  $10^6 M_\odot$  subhalo at 100 kpc, where  $\ln \Lambda \equiv \ln(b_{max}/b_{min}) \approx 10$  is the log of the ratio of the maximum and minimum impact distances (Binney & Tremaine 2008). Therefore, DF is negligible throughout our model.

*Disk Shocking:* Dehnen et al. (2004) found that the evolution of Pal-5 is driven by the tidal shocks when crossing the Galactic disk, which is not modeled in our simulations. The orbit of Pal-5 in Dehnen et al. (2004) has peri- and apogalacticon at 5.5 kpc and 19 kpc, respectively, whereas our smooth stream has peri- and apogalacticon at 15 kpc and 30 kpc, respectively. Being farther away from the Galactic center, if our simulations contained a disk, its effect should be less severe for our simulated stream than Pal-5. Moreover, Dehnen et al. (2004) concluded that disk shocking is not responsible for the observed structure in Pal-5, while Küpper et al. (2010) concluded that EOs persist even under the influence of disk shocks, so the absence of a disk should not significantly change our conclusion. The gap formation rate with and without subhalos in the presence of a disk is beyond the scope of this study.

*Halo Shape and Collapse History:* Siegal-Gaskins & Valluri (2008) found that the shape of the halo potential can have a larger effect than subhalos have on the overall structure of a stream. However, their simulations focused on streams which originated from DGs at  $\sim 10^9 M_\odot$ , as well as subhalos at  $\gtrsim 10^7 M_\odot$  which is the high end of our mass spectrum of subhalos. The small gaps from a stream originating from a GC in a non-spherical halo has yet to be studied. In fact, since the initial collapse of the entire halo, the potential cannot be stationary throughout a Hubble time, which is the timescale of our simulations. In the future, we aim to repeat a similar study using potentials which resulted directly from high resolution simulations such as Madau et al. (2008) and Springel et al. (2008). The self-consistent halo and subhalo potentials from those simulations can eliminate the idealized models in Section 2.1.

## 5. CONCLUSIONS

For the first time, we used N-body simulations to model the disruption of a collisionless star cluster which formed a narrow stream similar to Pal-5 and GD-1, and we investigated the phenomenology of gaps that originated from the perturbations by subhalos predicted in the  $\Lambda$ CDM cosmological model. Analytical predictions of stream gap statistics in previous studies were all based on massless particles distributed to mock realistic streams, but the dynamics of gaps have never been studied in self-consistent models. With a stream from a self-consistent model, we characterized the gap length distribution which can be used as a tool to understand the origin of stream gaps seen in observations.

The properties of the subhalos in our simulations were approximations to those in the Aquarius simulation (Springel et al. 2008). We ran 14 simulations of the same stream – 1 without any subhalos (the smooth stream), and 1 for each cumulative mass range in Table 1 (the  $\Lambda$ CDM streams). In each stream we looked for gaps using a matched filter approach previously used by Carlberg et al. (2012) and Carlberg & Grillmair (2013). We found that, in addition to subhalo perturbations, the overdensities of particles due to their epicyclic motions as the progenitor loses mass (Küpper et al. 2008) can also produce gaps. Therefore, even without subhalos, “gaps” can appear within  $\sim 5$  kpc away from the progenitor. For the first time, our match filter approach accounted for these EOs together with the gaps due to subhalo perturbations.

Yoon et al. (2011) first noted that subhalo gaps were typically diagonal and not perpendicular to the stream due to the range in angular momenta across the width of the stream. We investigated whether this could be a hindrance to gap detection. By measuring the distribution of angular momenta in our simulated stream, we estimated that the two ends of a gap across the width of a stream were sheared by no more than a 1 kpc per Gyr. Rather, subhalo gaps show complicated morphologies which were already imprinted into the stream as soon as the gaps first occurred. In addition to integrating the entire thickness of the stream, we also considered the case where the linear density are integrated using only the central 0.08 kpc of the stream in order to minimize the impact of gaps morphologies. We found that the resulting gap rate spectra the two cases were similar. Therefore, gap morphology does not affect our conclusion.

We tested the validity of the idealized gap spectrum  $R_{\cup}$ , or the cumulative number of gaps per unit stream length per unit stream age as a function of gap length  $l$ , derived by Carlberg (2012). We found that overlapping gaps in the stream can significantly reduce  $R_{\cup}$ , and that the dependences of  $R_{\cup}$  on subhalo masses and stream age are smaller than its dependence on the stream’s or-

bital phase. Therefore, the stream’s orbital phase must be known when interpreting gap formation rates in observations.

We considered how to interpret gap spectra from observations by projecting the stream onto the sky, and for each  $\Lambda$ CDM stream we also simulated them using ten realizations of the same subhalo distributions. One observational concern is the S/N of the stream’s detection. We down-sampled our simulated streams with less particles in order to match the S/N which is similar to the GD-1 detection (Carlberg & Grillmair 2013). Our result indicated that at GD-1’s S/N, the gap spectrum can be biased by the orbital phase of the stream. In addition, we compared gap spectra produced purely by EOs and by EOs and subhalos together in a  $\Lambda$ CDM halo. We showed that the gap spectra of the former are limited in gap lengths, and that the latter have a much larger variety of gap lengths. This can be a powerful method to identify the origin of gaps in streams. Therefore, high S/N data such as those from *Gaia* will be very useful for using stream gaps to constraint the abundance of subhalos.

The dynamics of stream gaps depend on the details of the dynamics of the stream itself. We adapted a few tools such as match filter and scaling relations which were derived from idealized simulations. In a future study, we aim to use self-consistent streams to repeat experiments akin to Yoon et al. (2011), Carlberg (2012), and Carlberg (2013), where the details of individual gaps can be studied in controlled experiments, in order to revise the aforementioned tools that is applicable quantitatively to realistic streams.

We thank the anonymous referee for valuable comments, which inspired us to expand the content of this paper. Computations were performed on the GPC supercomputer at the SciNet HPC Consortium. SciNet is funded by: the Canada Foundation for Innovation under the auspices of Compute Canada, the Government of Ontario; Ontario Research Fund - Research Excellence, and the University of Toronto.

## REFERENCES

- Bardeen, J. M. Bond, J. R., Kaiser, N., et al. 1986, ApJ, 304, 15  
 Barkana, R., Haiman, Z., & Ostriker, J. P. 2001, ApJ, 558, 482  
 Benson, A. J., Farahi, A., Cole, S. 2013, MNRAS, 428, 1774  
 Binney, J. & Tremaine, S. 2008, Galactic Dynamics (2nd ed.; Princeton, NJ: Princeton Univ. Press)  
 Blumenthal, G. R., Faber, S. M., Primack, J. R., et al. 1984, Nature, 311, 517  
 Bode, P., Ostriker, J. P., & Turok, N. 2001, ApJ, 556, 93  
 Bullock, J. S. 2010, arXiv:1009.4505  
 Carlberg, R. G. 2009, ApJ, 705, L223  
 Carlberg, R. G. 2012, ApJ, 748, 20  
 Carlberg, R. G. 2013, ApJ, 775, 95  
 Carlberg, R. G., & Grillmair C. J. 2013, ApJ, 768, 171  
 Carlberg, R. G., Grillmair C. J., & Hetherington N. 2012, ApJ, 760, 75  
 Comarretta, J., & Quillen, A. C. 2011, MNRAS, 414, 810  
 Davis, M., Efstathiou, G., Frenk, C. S., et al. 1985, ApJ, 292, 371  
 Dehnen, W., Odenkirchen, M., Grebel, E. K., et al. 2004, AJ, 127, 2753  
 Eyre, A., & Binney, J. 2011, MNRAS, 413, 1852  
 Gao, L., Frenk, C. S., Boylan-Kolchin, M., et al. 2011, MNRAS, 410, 2309  
 Grillmair, C. J. 2010, in Galaxies and Their Masks, ed. D. Block, K. C. Freeman, & I. Puerari (New York: Springer), 247  
 Grillmair C. J., & Dionatos O. 2006, ApJ, 643, L17  
 Harris, W. E. 1996, AJ, 112, 1487  
 Helmi A., White S. D. M., & Springel, V. 2003, MNRAS, 339, 834  
 Hernquist, L. 1990, ApJ, 356, 359  
 Ibata, R. A., Lewis, G. F., Irwin, M. J., et al. 2002, MNRAS, 332, 915  
 Johnston, K. V. 1998, ApJ, 495, 297  
 Just, A., Berzlik, P., Petrov, M. I., et al. 2009, MNRAS, 392, 969  
 Kamionkowski, M., & Liddle, A. 2000, PhRvL, 84, 4525  
 Klypin, A., Kravtsov, A. V., Valenzuela, O., et al. 1999, ApJ, 522, 82  
 Kposov, S. E., Rix H. W., & Hogg D. W. 2010, ApJ, 712, 260  
 Kposov, S. E., Yoo, J., Rix, H.-W., et al. 2009, ApJ, 696, 2179  
 Küpper, A. H. W., MacLeod, A., & Heggie D. C. 2008, MNRAS, 387, 1248  
 Küpper, A.H.W., Kroupa, P., Baumgardt, H., et al. 2010, MNRAS, 401, 105  
 Law D. R., Johnston K. V., & Majewski S. R. 2005, ApJ, 619, 807  
 Macciò A. V., Kang, X., Fontanot, F., et al. 2010, MNRAS, 402, 1995  
 Madau, P., Diemand, J., & Kuhlen, M. 2008, ApJ, 679, 1260  
 Moore, B., Ghigna, S., Governato, F., et al. 1999, 524, L19  
 Navarro, J. F., Frenk, C. S., & White S. D. M. 1997, ApJ, 490, 493

- Navarro, J. F., Hayashi, E., Power, C., et al. 2004, MNRAS, 349, 1039
- Navarro, J. F., Ludlow, A., Springel, V., et al. 2010 MNRAS, 402, 21
- Neto, A. F., Gao, L., Bett, P., et al. 2007, MNRAS, 381, 1450
- Odenkirchen, M., Grebel, E. K., Rockosi, C. M., et al. 2001, ApJ, 548, L165
- Odenkirchen, M., Grebel, E. K., Kayser, A., et al. 2009, AJ, 137, 3378
- Perlmutter, S., Aldering, G., Goldhaber, G., et al. 1999, ApJ, 517, 565
- Planck Collaboration, et al. 2013, arXiv:1303.5062
- Riess, A. G., Filippenko, A. V., Challis, P., et al. 1998, AJ, 116, 1009
- Schneider, A., Smith, R. E., & Reed, D. 2013, MNRAS, 433, 1573
- Siegal-Gaskins, J. M., & Valluri, M. 2008, ApJ, 681, 40
- Spergel D. N., & Steinhardt, P. J. 2000, PhRvL, 84, 3760
- Springel, V. 2005, MNRAS, 364, 1105
- Springel, V., Wang, J., Vogelsberger, M., et al. 2008, MNRAS, 391, 1685
- Stadel, J., Potter, D., Moore, B., et al. 2009, MNRAS, 398, L21
- Strigari, L. E., Bullock, J. S., Kaplinghat, M. 2007, ApJ, 669, 676
- Strigari, L. E., Bullock, J. S., Kaplinghat, M., et al. 2008, Nature, 454, 1096
- Willett, B. A., Newberg, H. Jo, Zhang, H., et al. 2009, ApJ, 697, 207
- Yoon, J. H., Johnston, K. V., & Hogg, D. W. 2011, ApJ, 731, 58
- Zemp, M., Diemand, J., Kuhlen, M., et al. 2009, MNRAS, 394, 641